

PET/MR imaging of bone lesions – implications for PET quantification from imperfect attenuation correction

Andrei Samarin · Cyrill Burger ·
Scott D. Wollenweber · David W. Crook ·
Irene A. Burger · Daniel T. Schmid ·
Gustav K. von Schulthess · Felix P. Kuhn

Received: 11 October 2011 / Accepted: 11 March 2012 / Published online: 14 April 2012
© Springer-Verlag 2012

Abstract

Purpose Accurate attenuation correction (AC) is essential for quantitative analysis of PET tracer distribution. In MR, the lack of cortical bone signal makes bone segmentation difficult and may require implementation of special sequences. The purpose of this study was to evaluate the need for accurate bone segmentation in MR-based AC for whole-body PET/MR imaging.

Methods In 22 patients undergoing sequential PET/CT and 3-T MR imaging, modified CT AC maps were produced by replacing pixels with values of >100 HU, representing mostly bone structures, by pixels with a constant value of 36 HU corresponding to soft tissue, thereby simulating current MR-derived AC maps. A total of 141 FDG-positive osseous lesions and 50 soft-tissue lesions adjacent to bones were evaluated. The mean standardized uptake value (SUV_{mean}) was measured in each lesion in PET images reconstructed once using the standard AC maps and once using the modified AC maps. Subsequently, the errors in lesion tracer uptake for the modified PET images were calculated using the standard PET image as a reference.

Results Substitution of bone by soft tissue values in AC maps resulted in an underestimation of tracer uptake in osseous and soft tissue lesions adjacent to bones of 11.2 ± 5.4 % (range 1.5–30.8 %) and 3.2 ± 1.7 % (range 0.2–4 %), respectively. Analysis of the spine and pelvic osseous lesions revealed a substantial dependence of the error on lesion composition. For predominantly sclerotic spine lesions, the mean underestimation was 15.9 ± 3.4 % (range 9.9–23.5 %) and for osteolytic spine lesions, 7.2 ± 1.7 % (range 4.9–9.3 %), respectively.

Conclusion CT data simulating treating bone as soft tissue as is currently done in MR maps for PET AC leads to a substantial underestimation of tracer uptake in bone lesions and depends on lesion composition, the largest error being seen in sclerotic lesions. Therefore, depiction of cortical bone and other calcified areas in MR AC maps is necessary for accurate quantification of tracer uptake values in PET/MR imaging.

Keywords PET · MR · Attenuation correction · Bone segmentation · CT simulation

A. Samarin · C. Burger · D. W. Crook · I. A. Burger ·
D. T. Schmid · G. K. von Schulthess · F. P. Kuhn
Department of Medical Radiology, University Hospital of Zurich,
Zurich, Switzerland

S. D. Wollenweber
GE Healthcare,
Waukesha, WI, USA

A. Samarin (✉)
Nuclear Medicine, University Hospital Zurich,
Rämistrasse 100,
8091 Zurich, Switzerland
e-mail: andsam@gmail.com

Introduction

Accurate attenuation correction (AC) is essential for quantitative analysis of PET tracer distribution, especially for assessing treatment response and comparing PET/MR to PET/CT data. AC of PET data based on MR images is challenging [1]. In contrast to CT data which can be easily transformed into attenuation coefficients for PET, intensity values in MR images do not reflect the X-ray density of tissues [2, 3]. Thus image processing of MR data is necessary for the generation of AC maps. Proposed approaches to

MR-based AC (MR AC) are tissue segmentation, the use of atlases or templates and pattern recognition techniques or a combination of these [4–7]. Tissue segmentation has worked well in PET/CT; however, the lack of cortical bone signal in currently available MR sequences makes bone segmentation difficult. A remedy might be provided by ultrashort or zero echo time sequences [8, 9].

There are no substantial clinical data showing whether it is necessary to segment bone in MR AC maps or whether the stronger attenuation of the 511 keV photons by bone can be replaced by the attenuation of soft tissue in such maps. Some investigators state that segmentation of CT images into three (background, lung and soft tissue) or four (background, lungs, fat and soft tissue) tissue classes to generate attenuation maps does not substantially change PET data compared to the use of standard CT AC with a mean underestimation of bone lesion SUV of 6.5 % and 8 %, respectively [5, 6]. In contrast, a recent study has shown that segmentation of whole-body CT data into four classes, while neglecting bone, results in SUV errors of >10 % in 58 % of osseous lesions [7]. All these studies evaluated the effects on a lesion by lesion basis, but did not consider that bone lesion density can vary considerably spanning from lytic to sclerotic.

In order to better understand the effects of bone attenuation using MR AC without bone segmentation, we generated whole-body error maps using CT data that allowed us to visualize the areas of the body in which the resulting errors from ignoring bone in AC were substantial or were only minimal. Additionally, this approach allowed determination of the systematic error in PET/MR compared to PET/CT when neglecting bone for MR AC. Approaches for correcting for such errors may be necessary because some patients will undergo PET/MR and PET/CT examinations interchangeably for therapy monitoring in the future.

Errors in SUV from MR AC ignoring bone not only depend on the body region, but also on the density of the bone lesions themselves. This in turn depends on the underlying disease process and may change significantly during the course of a disease or after therapy. Frequently bone lesions are initially lytic, but on follow-up examinations the bone lesions may become sclerotic. These changes in lesion density will not be evident when treating bone as soft tissue in MR AC maps. The influence of the composition of bone lesions on the errors in SUV in segmented AC approaches has not been studied before.

The purpose of this study was therefore twofold: to generate error maps to estimate the accuracy of bone segmentation in MR AC for whole-body PET/MR imaging and to specifically look at errors in bone lesions of various compositions and lesions close to bone.

Materials and methods

Patients

This institutional review board-approved retrospective study included 22 patients with osseous lesions and soft-tissue lesions adjacent to bone who were selected from a total of 120 patients. All 22 patients underwent sequential PET/CT and 3-T MR imaging between December 2010 and June 2011 as part of a clinical/research work-up. In this study, only the PET/CT part of the studies was used. The patient characteristics are summarized in Table 1.

Image acquisition

PET/CT imaging was performed on a full-ring, state-of-the-art time-of-flight PET/CT system (Discovery PET/CT 690; GE Healthcare). Patients fasted for at least 4 h prior to injection of a dose of 360.7 ± 18 of ^{18}F -FDG (Table 1). After an uptake time of 60 min, native low-dose CT data and PET emission data were acquired from the mid-thigh to the vertex of the skull. CT data were acquired with 50–79 mAs per slice, 120 kVp, a pitch of 0.984:1, a collimation of 64×0.625 mm, a measured FOV of 50 cm and a noise index of 20 %, and were reconstructed to images of 0.625 mm transverse pixel size and 3.75 mm slice thickness. PET data were acquired in 3-D mode with a fixed scan duration of 2 min and an axial FOV of 153 mm per bed position. Seven axial FOVs were used.

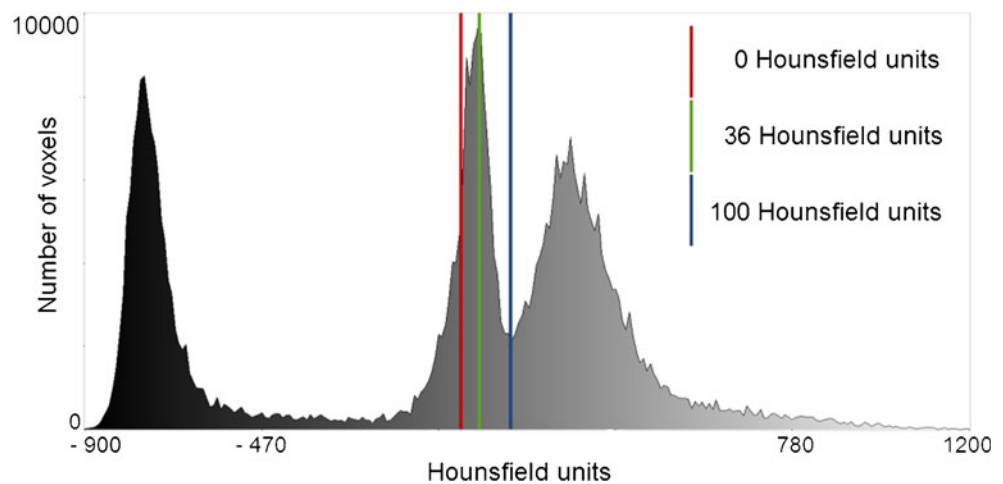
Reconstruction of attenuation maps

In each patient standard and modified CT AC maps were generated by a trilinear transformation of non-enhanced low-dose CT images to 511 keV PET attenuation maps [2]. According to the performed histogram analysis of CT images (Fig. 1) the density cut-off for the bone tissue segmentation was defined as 100 HU while the representative density value for the soft tissue was set at 36 HU. Modified AC maps (AC-Mod) were produced using PMOD software (PMOD Technologies, Zurich, Switzerland) by replacing pixels with values higher than 100 HU by pixels with a

Table 1 Patient characteristics

Characteristic	Value
Number of patients	22
Age (years, mean \pm SD)	58.2 \pm 14.9
Weight (kg, mean \pm SD)	75.3 \pm 8.4
Male	16 (73 %)
^{18}F -FDG dose (MBq, mean \pm SD)	360.7 \pm 18
^{18}F -FDG uptake time (min, mean \pm SD)	62.2 \pm 3.6

Fig. 1 Histogram analysis of CT images. The density cut-off for bone tissue segmentation was defined based on this histogram as 100 HU while that for soft tissue was set at 36 HU



constant value of 36 HU, thereby simulating substitution of bone by soft tissue in MR-derived segmented AC maps. Standard AC maps (AC-St) were produced from the same but unmodified non-enhanced low-dose CT images. Hounsfield units were transformed into 511 keV attenuation using the following algorithm: $AC [1/cm] = \text{intercept} + CT \text{ value} * \text{slope}$. CT values below 50 HU were converted to attenuation using the kVp-independent soft-tissue conversion with an intercept of 0.096 and a slope of 9.6×10^{-5} . CT values of 50 HU and above were converted using the 120-kVp bone scale with an intercept of 0.0982 and a slope of 5.11×10^{-5} . Subsequently, two sets of attenuation-corrected PET images were reconstructed based on the modified and standard AC maps. An overview of the image reconstruction procedure is given in Fig. 2.

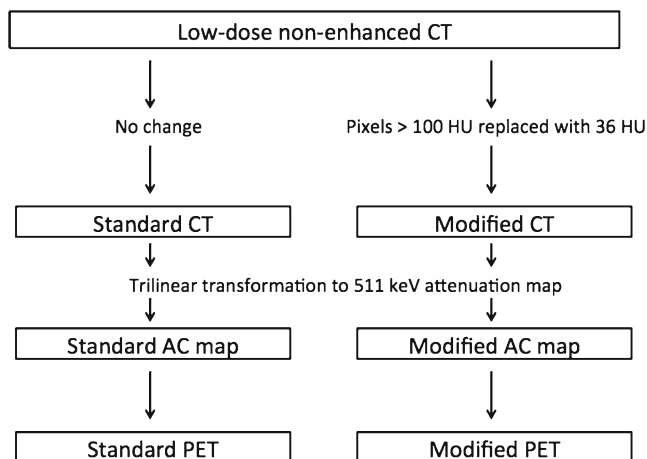


Fig. 2 Generation of AC maps followed by PET data reconstruction. The modified CT data were generated by replacing all pixels in CT sections with values >100 HU by pixels with a value of 36 HU. The “no-bone” CT data obtained were then used for AC of PET images and compared to the PET images which were AC-corrected in standard mode

Generation of a whole-body SUV error map

Whole-body maps showing the percentage differences in SUV between PET images reconstructed using the modified AC map (PET_{AC-Mod}) and the standard AC map (PET_{AC-St}) were generated using the following formula: $(PET_{AC-Mod} - PET_{AC-St}) / PET_{AC-St} \times 100 \%$. The resulting difference map was analysed for body regions showing the largest differences in SUV.

Image analysis

First, the mean SUV of FDG avid lesions located in bone and in soft tissues adjacent to bone (within 10 mm) were measured by placing a volume of interest of 10 mm diameter on PET_{AC-St} and PET_{AC-Mod} images. The volume of interest was placed within PET-positive lesions of at least 1 cm^3 . Subsequently, the standard error of SUVmean in the lesions was calculated for the PET_{AC-Mod} images using the PET_{AC-St} images as a reference. SUVmean rather than SUVmax was measured because recent literature suggests that reporting SUVmean gives results closer to reality than SUVmax [10, 11]

Bone lesions were then divided into lesions involving spine, pelvic bones and other bones. Spine and pelvic lesions were further classified into three classes based on their appearance on CT images: (1) lytic lesions showing predominant and clearly visible destruction of osseous matrix with CT density below 100 HU, (2) sclerotic lesions showing predominantly increased bone density with CT density above 200 HU, and (3) lesions of mixed density showing a combination of destructive and sclerotic changes or lesions without visible change in bone density on CT images with a CT density in the range 100–200 HU. The means and standard errors were similarly calculated for these classes as for all bone lesions and for the various anatomic locations (Table 2).

Table 2 Summary of SUV underestimation produced by reconstruction of PET images using modified AC maps

Location	Number of lesions	Mean error \pm SD (%)	Minimum error (%)	Maximum error (%)
Spine, vertebral bodies				
Sclerotic	23	15.9 \pm 3.4	9.9	23.5
Mixed density	13	10.6 \pm 1.5	8.7	11.2
Lytic	7	7.2 \pm 1.7	4.9	9.3
Pelvic bones				
Sclerotic	17	14.2 \pm 4	8.4	23.8
Mixed density	15	13.1 \pm 4.9	6.2	21.3
Lytic	9	6.8 \pm 2.7	3.1	12
Spine, vertebral processes				
Sacrum	4	9.6 \pm 3.8	4.9	13.9
Sternum	11	8.6 \pm 4.6	4.3	19.6
Sternum	7	8.5 \pm 2.5	4.8	11.3
Ribs	10	3 \pm 1	1.5	4.8
Scapula	3	7.7 \pm 3.3	4.8	11.1
Humerus	11	8.4 \pm 3	4	11
Femur	11	16.8 \pm 7	9.5	30.8
Total bone lesions	141	11.2 \pm 5.4	1.5	30.8
Soft-tissue lesions located near bone	50	3.2 \pm 1.7	0.2	4

Results

Analysis of the whole-body error maps showed that the largest errors with an average of 15–20 % were present in bone (Figs. 3 and 4). In the soft tissues the highest SUV errors were seen in the brain and tissues just adjacent to the bones (10–15 %) with a rapid decrease in error magnitude with distance from bone. Errors in other areas of the body SUV error maps were generally below 5 %. In addition to areas of underestimation, regions of slight overestimation of SUV were also identified in soft tissue on the SUV error maps (Fig. 3), but again not exceeding 5 %. Bone lesions and soft-tissue lesions adjacent to bone were quantitatively assessed for SUV errors (Table 2). Quantitative analysis of brain lesions was not

performed as the focus was on body imaging and our series contained only a single patient with a brain lesion. In Fig. 4, axial images of a fusion of SUV error maps and original CT images are shown with colour codes giving error ranges.

A total of 141 FDG-positive osseous lesions were found in 13 patients including 43 lesions in the vertebral bodies of the thoracic and lumbar spine, 41 lesions in the pelvic bones and 57 lesions in other bones. Further analysis of the density of vertebral body lesions on CT images revealed 23 sclerotic, 13 with normal or mixed density and 7 lytic lesions. In the pelvis, 17 sclerotic, 15 normal or mixed density and 9 lytic lesions were found.

Substitution of bone by soft tissue density values in AC maps resulted in a mean underestimation of SUV in all bone

Fig. 3 Example whole-body error maps in the sagittal (a) and coronal (b) planes showing the difference in percentage SUV between PET images reconstructed using modified AC maps treating bone as soft tissue and standard AC maps. Error maps were generated using the following formula: $(PET_{AC-Mod} - PET_{AC-St}) / PET_{AC-St} \times 100\%$. While most areas show SUV underestimation (blue), there are also some areas of slight SUV overestimation (red)

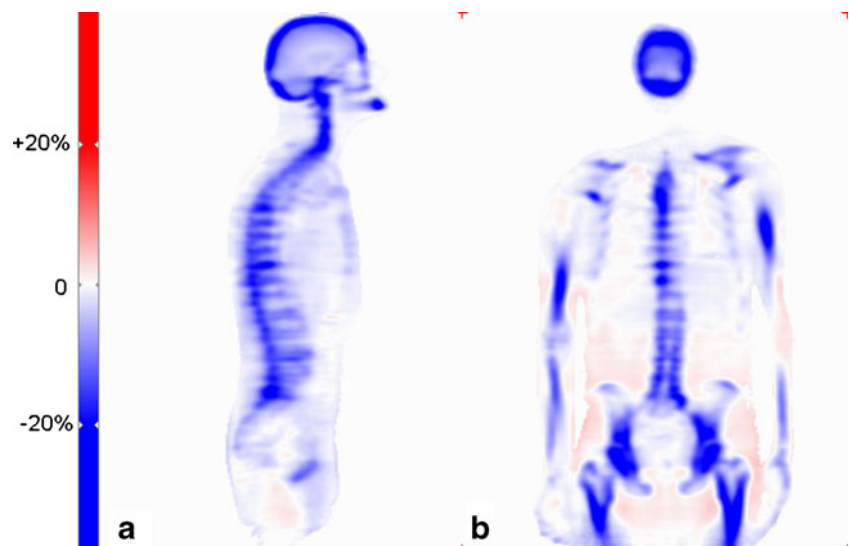
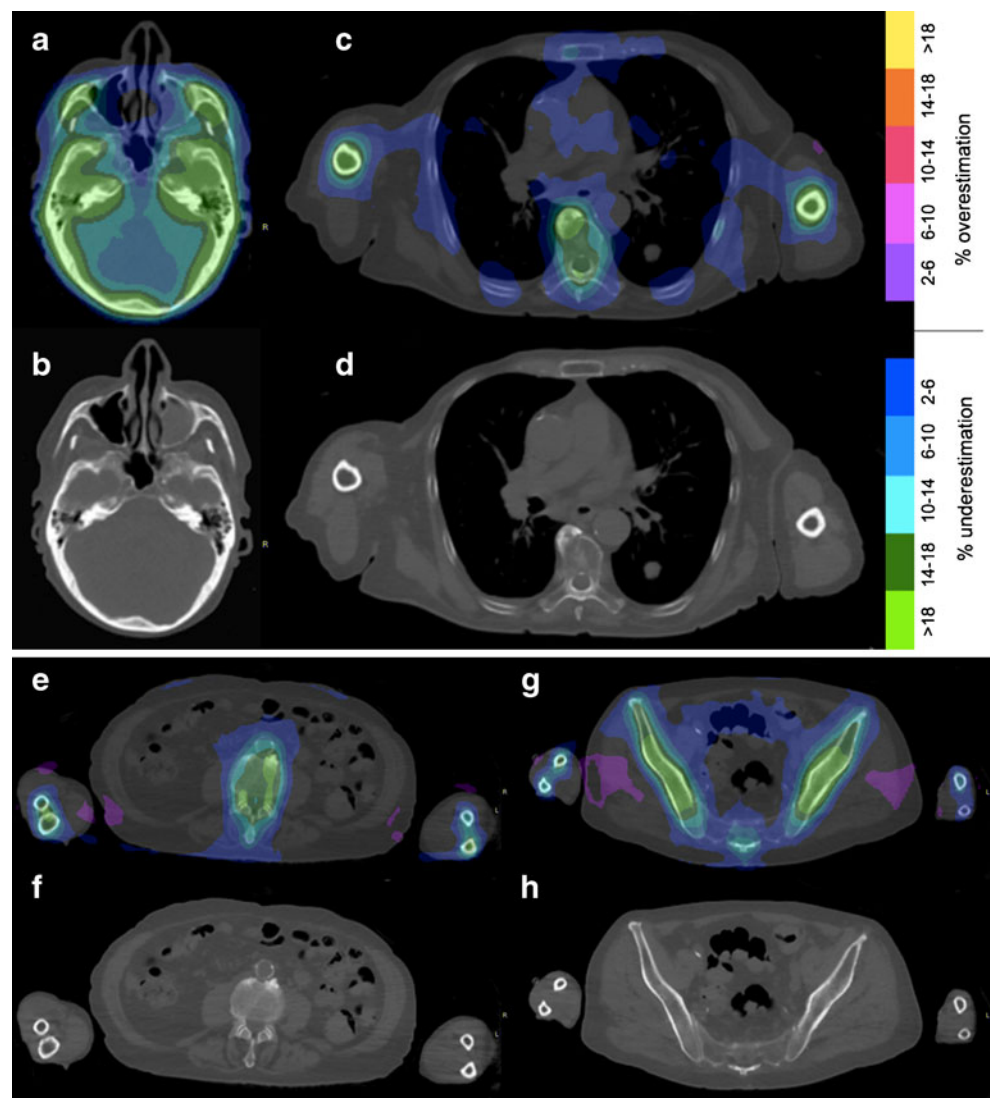


Fig. 4 Example axial images through the base of the skull (a, b), chest (c, d), abdomen (e, f) and pelvis (g, h) showing fusion of SUV error maps and original CT images. The largest underestimation in SUV is seen in bone and rapidly decreases from soft tissue adjacent to bone (within 10 mm) to more distant soft tissue. Of note, the error is substantially larger in a dense osteophyte in the right anterior aspect of the thoracic vertebral body shown (c, d) compared to the other parts of the vertebral body



lesions of 11.2 ± 5.4 %. A minimum SUV underestimation of 1.5 % was seen in a rib lesion while a maximum SUV underestimation of 30.8 % was identified in a sclerotic lesion located in the femoral bone. A summary of SUV errors in bone lesions of different composition in various regions produced by reconstruction of PET images using the modified AC maps is given in Table 2.

Analysis of 52 spine and 41 pelvic lesions revealed an important dependence of the underestimation error on the composition of the lesions, while this error was substantially smaller in other lesions and thus not further analysed. For predominantly sclerotic, normal/mixed density and lytic lesions of the thoracic and lumbar spine vertebral bodies, the underestimation errors were 15.9 ± 3.4 % (mean \pm SD, range 23.5–9.9 %), 10.6 ± 1.5 % (range 11.2–8.7 %) and 7.2 ± 1.7 % (range 9.3–4.9 %), respectively. For osseous lesions in the pelvis, the corresponding underestimation errors for sclerotic, normal/mixed density and lytic lesions were

14.2 ± 4 % (range 23.8–8.4 %), 13.1 ± 4.9 % (range 21.3–6.2 %) and 6.8 ± 2.7 % (range 12–3.1 %), respectively.

A total of 50 FDG-positive lesions were identified in the soft tissues adjacent to bony structures in six patients. In these lesions, substitution of the bone by soft tissue values in the AC maps resulted in underestimation errors of 3.2 ± 1.7 % (mean \pm SD). Among these lesions, the smallest error of 0.2 % was found in a lung lesion adjacent to a rib, while the largest error of 4 % was seen in a lymph node adjacent to the osseous pelvis.

Discussion

Decreases in SUV were highest for lesions within or next to bone when PET images were reconstructed using a modified AC map treating bone as soft tissue versus a standard AC map. The magnitude of this error decreased rapidly with the distance

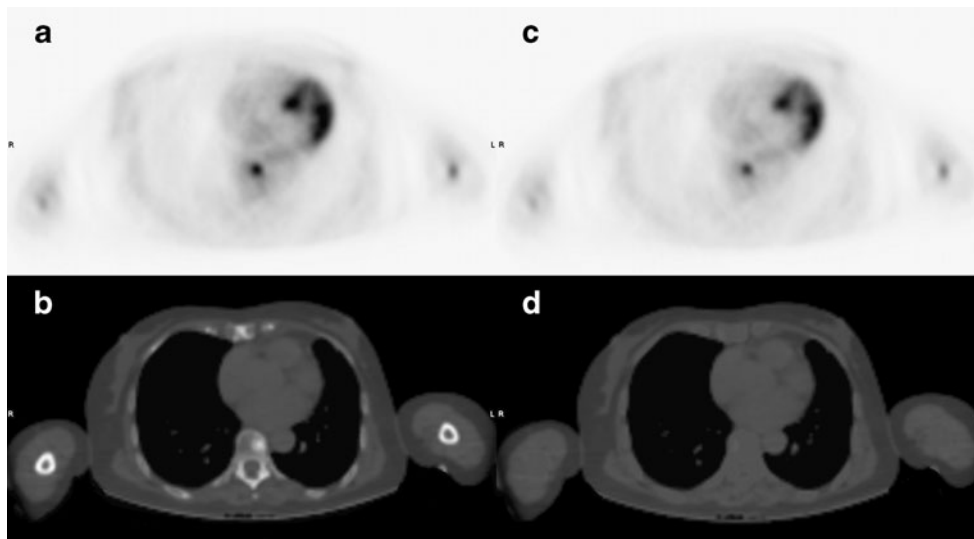


Fig. 5 A 70-year-old woman with a sclerotic bone metastasis of breast cancer in thoracic vertebral body 10. **a** PET image reconstructed using the standard CT AC map shows an FDG-avid lesion in the left anterior aspect of T10. **b** Standard CT AC map shows that the bone lesion is sclerotic. **c**

PET image reconstructed using the modified CT AC map. **d** In the modified CT AC map bone is substituted by soft tissue. In this case modification of the AC map has resulted in underestimation of FDG uptake by 23 % in this bone metastasis in the modified PET image

form bone and showed only a very small difference in other areas of the body (brain not analysed in this study). Therefore 191 lesions, 141 in bone and 50 adjacent to bone were examined in more detail. Based on the analysis of the 141 FDG-positive bone lesions, substitution of bone by soft tissue in AC maps for PET resulted in average underestimation of SUV in bones by around 10 %. Lesions located in the ribs showed an average error below 5 %, while lesions located in the proximal femur showed a larger average error of more than 15 %. Importantly, in our study the maximum SUV underestimation for bone lesions of more than 20 % was seen in dense sclerotic lesions: 23.5 % for spine lesions, 23.8 % for pelvic bone lesions and 30.8 % for femoral lesions.

Compared to the studies performed by Martinez-Möller et al. [5] (21 osseous lesions with an average SUV change of 8 ± 3 % and maximal underestimation of 13.1 % seen in a lesion in the pelvic bone) and by Schulz et al. [6] (7 bone lesions with an average underestimation of 6.5 ± 4.1 % and maximum error of -13.4 % seen in a pelvic bone lesion), the average and maximum errors seen in osseous lesions were significantly higher in our study. The results of our study support the findings of Hofmann et al. which showed tracer uptake quantification errors of >10 % in 58 % of osseous lesions and errors >20 % in 22 % of the lesions [7]. The difference in the magnitude of underestimation may be explained by the larger number of osseous lesions examined in our study (141), and their location and composition. Additionally, another important factor may be the different approaches to reconstruction of the AC maps as we substituted only bone by soft tissue values rather than using a full three- or four-class CT segmentation. This approach allowed us to determine the effect of bone attenuation by changing only one parameter.

The errors observed are of interest for understanding the systematic errors in MR AC-based PET scans, but are particularly relevant when comparing the data obtained from PET/CT and PET/MR for treatment response assessment. In fact, an AC-induced 20–30 % error in SUV of a lesion might change the assessment of treatment response.

To our knowledge this is the first study showing a substantial difference in underestimation of SUV in PET between dense sclerotic and destructive lytic bone lesions when neglecting the bone in AC maps. The presence of 52 spine and 41 pelvic bone lesions allowed us to assess the dependence of the error on the density of the bone lesions. We found a substantial difference in SUV underestimation between the sclerotic lesions with an average error of -15.9 % in spine and -14.2 % in pelvic lesions and lytic lesions with respective underestimation values of -7.2 % and -6.8 %. The commonly used approach to MR-based AC is tissue segmentation with substitution of bone by soft tissue values [5–7, 12, 13]. In bone lesions with little or no change in density over the therapeutic course, this type of segmentation will result only in a systematic under-correction of bone attenuation between consecutive PET/MR scans and interpretation is not truly affected. However, the density of the bone lesions can change significantly during the course of the disease—and this will have an impact on their attenuation properties. Treating bone as soft tissue in the MR AC maps of consecutive PET/MR scans performed for assessment of treatment response may result in SUV differences solely due to changes in lesion density and not due to a change in the metabolic activity of the lesion.

The magnitude of the SUV error of bone lesions is dependent not only on their own density but also on the density of the surrounding bones, being smaller in osteoporotic bones and

larger in the presence of degenerative changes or in certain disease states (e.g. myelofibrosis, mastocytosis, osteopetrosis).

Analysis of whole-body SUV error maps also revealed an underestimation of tracer uptake in soft tissues adjacent to bone. Dedicated analysis of 48 soft tissue lesions in close proximity to bone revealed that the errors were lower than 5 % (mean underestimation 3.2 %, maximum 4 %), which for clinical purposes may be negligible. While our data do not allow the relevance of skull bone for the AC of brain lesions to be addressed, other authors have shown that this is mandatory to quantify brain PET examinations [14]. In addition to the SUV underestimation highlighted above, minor SUV overestimation was also seen in some soft tissue regions. This is potentially due to differences caused by the interaction between changes in attenuation and the scatter correction of the data, but again is hardly clinically relevant.

In agreement with lesion-based evaluations of other studies [5, 6], our AC maps suggest that for lesions in soft tissues, fat or lung, the omission of bone from the AC of PET data is clinically not relevant, at least at the levels of accuracy at which SUV values are used nowadays. However, neglecting bone can lead to relatively high SUV errors in lesions within bone, especially in sclerotic areas. Therefore, in PET/MR, the application of MR sequences able to depict bone might be necessary not only for MR AC in brain tissue, but also for lesions within bone throughout the body. In such lesions we have no a priori knowledge without CT data if they are lytic, sclerotic or mixed, and this can change during the course of a disease, making therapy monitoring challenging when using MR AC ignoring attenuation by bone.

Conclusion

Treating bone as soft tissue in MR-derived AC maps for PET/MR leads to a substantial underestimation of SUV values in bone lesions. The errors depend substantially on lesion composition, with the largest error being seen in sclerotic lesions. Therefore depiction of the cortical bone and sclerotic areas in MR AC maps is necessary for accurate quantification of tracer uptake values in whole-body PET/MR imaging.

Acknowledgments The authors thank Albert Lonn for useful discussions.

Research support This work was supported in part by a research grant from GE Healthcare, Waukesha, WI, USA.

Conflicts of interest One of the authors (S.W.) is an employee of GE HealthCare, Waukesha WI, USA. The research group receives research support from GE Healthcare.

References

- Hofmann M, Pichler B, Scholkopf B, Beyer T. Towards quantitative PET/MRI: a review of MR-based attenuation correction techniques. *Eur J Nucl Med Mol Imaging*. 2009;36 Suppl 1:S93–S104. doi:10.1007/s00259-008-1007-7.
- Burger C, Goerres G, Schoenes S, Buck A, Lonn AH, Von Schulthess GK. PET attenuation coefficients from CT images: experimental evaluation of the transformation of CT into PET 511-keV attenuation coefficients. *Eur J Nucl Med Mol Imaging*. 2002;29(7):922–7. doi:10.1007/s00259-002-0796-3.
- Beyer T, Weigert M, Quick HH, Pietrzyk U, Vogt F, Palm C, et al. MR-based attenuation correction for torso-PET/MR imaging: pitfalls in mapping MR to CT data. *Eur J Nucl Med Mol Imaging*. 2008;35(6):1142–6. doi:10.1007/s00259-008-0734-0.
- Hofmann M, Steinke F, Scheel V, Charpiat G, Farquhar J, Aschoff P, et al. MRI-based attenuation correction for PET/MRI: a novel approach combining pattern recognition and atlas registration. *J Nucl Med*. 2008;49(11):1875–83. doi:10.2967/jnumed.107.049353.
- Martinez-Möller A, Souvatzoglou M, Delso G, Bundschuh RA, Chef'd'hotel C, Ziegler SI, et al. Tissue classification as a potential approach for attenuation correction in whole-body PET/MRI: evaluation with PET/CT data. *J Nucl Med*. 2009;50(4):520–6. doi:10.2967/jnumed.108.054726.
- Schulz V, Torres-Espallardo I, Renisch S, Hu Z, Ojha N, Bornert P, et al. Automatic, three-segment, MR-based attenuation correction for whole-body PET/MR data. *Eur J Nucl Med Mol Imaging*. 2011;38(1):138–52. doi:10.1007/s00259-010-1603-1.
- Hofmann M, Bezrukov I, Mantlik F, Aschoff P, Steinke F, Beyer T, et al. MRI-based attenuation correction for whole-body PET/MRI: quantitative evaluation of segmentation- and atlas-based methods. *J Nucl Med*. 2011;52(9):1392–9. doi:10.2967/jnumed.110.078949.
- Keereman V, Fierens Y, Broux T, De Deene Y, Lonnewux M, Vandenberghe S. MRI-based attenuation correction for PET/MRI using ultrashort echo time sequences. *J Nucl Med*. 2010;51(5):812–8. doi:10.2967/jnumed.109.065425.
- Robson MD, Bydder GM. Clinical ultrashort echo time imaging of bone and other connective tissues. *NMR Biomed*. 2006;19(7):765–80. doi:10.1002/nbm.1100.
- Schwartz J, Humm JL, Gonen M, Kalaigian H, Schoder H, Larson SM, et al. Repeatability of SUV measurements in serial PET. *Med Phys*. 2011;38(5):2629–38.
- Burger IA, Huser DM, Burger C, von Schulthess GK, Buck A. Repeatability of FDG quantification in tumor imaging: averaged SUVs are superior to SUVmax. *Nucl Med Biol*. 2012; in press. doi:10.1016/j.nucmedbio.2011.11.002.
- Schleyer PJ, Schaeffter T, Marsden PK. The effect of inaccurate bone attenuation coefficient and segmentation on reconstructed PET images. *Nucl Med Commun*. 2010;31(8):708–16. doi:10.1097/MNM.0b013e32833b0573.
- Eiber M, Martinez-Moller A, Souvatzoglou M, Holzapfel K, Pickhard A, Loffelbein D, et al. Value of a Dixon-based MR/PET attenuation correction sequence for the localization and evaluation of PET-positive lesions. *Eur J Nucl Med Mol Imaging*. 2011;38(9):1691–701. doi:10.1007/s00259-011-1842-9.
- Catana C, van der Kouwe A, Benner T, Michel CJ, Hamm M, Fenchel M, et al. Toward implementing an MRI-based PET attenuation-correction method for neurologic studies on the MR-PET brain prototype. *J Nucl Med*. 2010;51(9):1431–8. doi:10.2967/jnumed.109.069112.